Journal of Materials Chemistry A

PAPER

View Article Online
View Journal | View Issue

Cite this: J. Mater. Chem. A, 2014, 2, 9405

Limiting factors for photochemical charge separation in $BiVO_4/Co_3O_4$, a highly active photocatalyst for water oxidation in sunlight†

Jiarui Wang and Frank E. Osterloh*

Received 4th April 2014
Accepted 29th April 2014

DOI: 10.1039/c4ta01654h

www.rsc.org/MaterialsA

Chemical modification of $BiVO_4$ nanoparticles (Scheelite, $E_G = 2.62$ eV) with chemically deposited Co_3O_4 nanoparticles improves the photocatalytic water oxidation activity by a factor of 17 to 11 mmol g^{-1} h^{-1} under visible light (AQE 10% at 435 nm) and to 1.24 mmol g^{-1} h^{-1} under sunlight from aqueous 0.02 M $NaIO_4$. This activity ranks among the highest among known visible light driven water oxidation photocatalysts. Based on systematic electrochemical, photoelectrochemical, and surface photovoltage measurements, the high photocatalytic activity can be attributed to the electrocatalytic properties of the Co_3O_4 cocatalyst and to the formation of a heterojunction at the $BiVO_4$–Co_3O_4 interface.

Introduction

The photocatalytic water splitting reaction is a carbon-free pathway to generate hydrogen fuel from abundant sunlight and water. Potentially, powdered catalysts[1–3] are the most economical way to drive this process.[4] Due to its chemical stability, 2.4 eV band gap, and n-type character, bismuth vanadate is a promising photoanode material for water oxidation – one half reaction in water photoelectrolysis.[5] Since its first mention in 1998 by Kudo *et al.*,[6] several structure types and morphologies of $BiVO_4$ have been reported for water oxidation.[7–11] It also has been established that the efficiency of unmodified $BiVO_4$ is limited by electron–hole recombination, slow carrier transport, and slow water oxidation kinetics.[12,13] Doping with molybdenum[14,15] or tungsten,[16] addition of cocatalysts Co–Pi,[15,17,18] FeOOH,[19] nanostructuring[19,20] and junction formation[5] have been explored to address these problems. In 2006, Long *et al.* reported that the addition of Co_3O_4 to $BiVO_4$ increased the activity for *phenol oxidation*.[10,21] As we show here, the addition of Co_3O_4 also leads to 17 times improved photocatalytic *water oxidation* with $BiVO_4$. After optimization of the Co_3O_4 content, suspended $BiVO_4$–Co_3O_4 (1%) composite particles catalyze water oxidation under visible light (380 mW cm^{-2}, 11 mmol g^{-1} h^{-1}) and direct sunlight (1.24 mmol g^{-1} h^{-1}). The quantum efficiency is 10% at 435 nm. Surface photovoltage spectra and electrochemical and photoelectrochemical data show that the improved performance can be attributed to the reduction of the water oxidation potential by Co_3O_4 [10,22] and to the formation of a $BiVO_4$–Co_3O_4 junction that aids electron–hole separation, and that creates a photovoltage of about 12 mV. This work sheds light on the importance of the light absorber–cocatalyst interfaces for achieving optimal charge separation in suspended water oxidation photocatalysts.

Results and discussion

Electron micrographs of $BiVO_4$ particles (Details in ESI†), made by solid-solution reaction and after calcination at 673 K[23] are shown in Fig. 1A. The particles have round features and sizes of 73 ± 35 nm and they are clustered into agglomerates. X-ray diffraction suggests the presence of the monoclinic Scheelite phase (Fig. S1†).

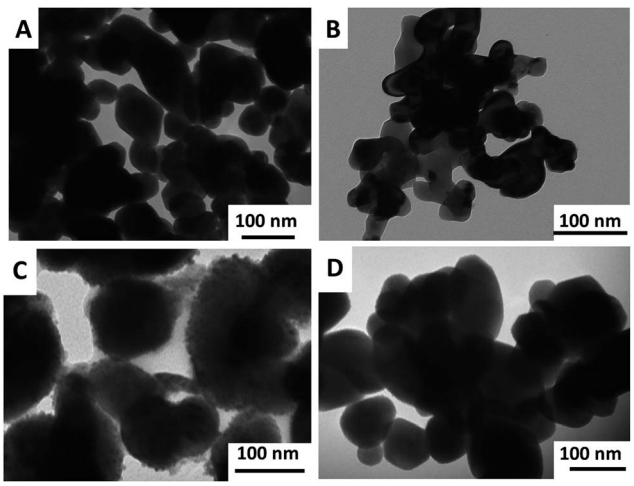

Fig. 1 TEM images of (A) $BiVO_4$, (B) commercial Co_3O_4 particles (C) Chem-Co_3O_4–$BiVO_4$ and (D) Phys-Co_3O_4–$BiVO_4$.

Department of Chemistry, University of California, Davis, USA. E-mail: fosterloh@ucdavis.edu

† Electronic supplementary information (ESI) available: X-ray diffraction patterns, SEM images overview of oxygen evolving photocatalysts, Butler–Ginley calculation of flat-band potentials, comparison of oxygen evolution catalysts and calculation of sun light intensity. See DOI: 10.1039/c4ta01654h

The optical properties of $BiVO_4$ and the composites are summarized in Fig. 2. The indirect and direct band gap of $BiVO_4$ was found as 2.45 eV and 2.62 eV by Tauc plot. This value is close to earlier reported 2.5 eV.[23] The introduction of the Co_3O_4 phase leads to a grey-yellow appearance of Chem-Co_3O_4–$BiVO_4$, which is due to a broad absorption at 500–900 nm (Fig. 2A) characteristic of the Co_3O_4 phase.[18] For Phys-Co_3O_4–$BiVO_4$, this absorption is obscured by scattering.

As will be shown in the following, $BiVO_4$–Co_3O_4 is an active photocatalyst for water oxidation in the presence of a chemical or electrochemical bias. In order to find the optimum Co_3O_4 content, a series of Co_3O_4–$BiVO_4$ samples were synthesized *via* an electrochemical route. Here, $BiVO_4$ electrodes were first prepared by drop-coating of the $BiVO_4$ powder on FTO coated glass substrates, and variable amounts (0.5, 1, 2 and 4 wt%) of cobalt metal were electrochemically deposited from 0.01 M $Co(NO_3)_2$ solution at a fixed current density of 0.2 mA cm^{-2}. The electrodes were then rinsed with water, dried in air and calcined at 673 K for 5 hours to oxidize the cobalt to Co_3O_4, and to produce thin films of composites, labeled as Echem-Co_3O_4–$BiVO_4$ in the following. Electrochemical scans of the Echem-Co_3O_4–$BiVO_4$ samples are shown in Fig. 3A. All materials have much lower water oxidation potentials at 1 mA cm^{-2} (1.35 V to 1.6 V *vs.* NHE) than unmodified $BiVO_4$ (2.38 V *vs.* NHE). This clearly showed that the added Co_3O_4 is an effective cocatalyst for water oxidation. The effect was most pronounced for the 4% Co_3O_4 containing sample, but even at 0.5% Co_3O_4 a significant 0.9 V decrease of the water oxidation overpotential was observed.

To evaluate the effect of the Co_3O_4 cocatalyst on photoelectrochemical water oxidation, the photocurrent response of the Echem-Co_3O_4–$BiVO_4$ films was measured in 0.1 M K_2SO_4 aqueous solution (Fig. 3B) under illumination from 435 nm LED (7.4 mW cm^{-2}). All samples produce anodic photocurrents at applied potentials above +0.5 V (NHE). The addition of Co_3O_4 first *decreases* the photocurrent (at 0.5% loading), then increases it at intermediate loading (1%), and then decreases it again at large loadings (2, 4%). Also, there are strong capacitive currents in the Co_3O_4 rich samples, as evident from the saw-tooth shape of the photocurrent response after switching the light. A magnified view of this current is shown in Fig. 3C in the time domain. It can be explained with the model shown in the insert of Fig. 3C. The capacitive charge Q is due to the trapping and detrapping of photogenerated charge carriers in the asymmetric Co_3O_4–$BiVO_4$–FTO configuration. The charging is driven by the photopotential U that develops across the illuminated film. Only some of the photoholes are able to generate a faradic current due to water oxidation, while the remainder flows back into the $BiVO_4$ film when the light is turned off. The reduced faradaic photocurrents for the films with the highest Co_3O_4 loading can simply be explained from the shading effect of the Co_3O_4 layer.

In contrast, Chem/Phys-Co_3O_4–$BiVO_4$ catalyst samples prepared by chemical or physical deposition of Co_3O_4 showed much cleaner photochemistry (Fig. 3D). In both photocurrent traces, the positive effect of the added Co_3O_4 can be observed clearly. The Co_3O_4 cocatalyst works as the hole collector and provides a fast path for the charge transfer between the $BiVO_4$ light absorber and the solution. No capacitive currents are observed due to homogeneous mixing of the Co_3O_4 phase with the $BiVO_4$ film.

Based on the photoelectrochemical data, suspensions of Co_3O_4–$BiVO_4$ should catalyze water oxidation when illuminated in the presence of a chemical bias. Accordingly, 50 mg of each catalyst were suspended in 50 mL of aqueous 0.05 M $AgNO_3$ (E^0 = 0.80 V NHE)[24] or 0.02 M $NaIO_4$ (E^0 = 1.60 V NHE),[25] and irradiated with visible light (Xe lamp, 380 mW cm^{-2}, >400 nm). Both reagents promote light-induced oxygen formation (Fig. 4A) at comparable rates, but in the presence of $AgNO_3$ the activity quickly falls off to zero. This is due to chemical deposition of silver metal, which also produces a dark grey coloration and aggregation of the sample. On the other hand, the rate of $NaIO_4$ sample stays constant during the eight-hour experiment and reaches 620 μmol g^{-1} h^{-1}. No O_2 was evolved in dark or when $NaIO_4$ was illuminated with Co_3O_4 only.

Fig. 4B shows a comparison of O_2 evolution from $BiVO_4$, Chem-Co_3O_4–$BiVO_4$ and Phys-Co_3O_4–$BiVO_4$. The reactivity increases in the order $BiVO_4$ (blue) < Phys-Co_3O_4–$BiVO_4$ (black) < Chem-Co_3O_4–$BiVO_4$ (red). Within 2 hours, the $NaIO_4$ is used up, and replaced with fresh reagent to fully re-establish O_2 production, without any decrease in activity. For the third run, the rate was calculated to be 11 mmol g^{-1} h^{-1}, which is 17 times greater than for unmodified $BiVO_4$. This activity ranks among the highest among known visible light driven water oxidation photocatalysts (Table S1†). The turnover number was 189 (based on $BiVO_4$) for the three tests, and the apparent quantum efficiency (AQE) is 10% at 435 nm (Fig. 4C) based on the data from 0.45 h in the 0.5–2.0 h interval (red box). The Co_3O_4–$BiVO_4$ catalyst was also tested under sunlight in Davis, CA to yield O_2 at

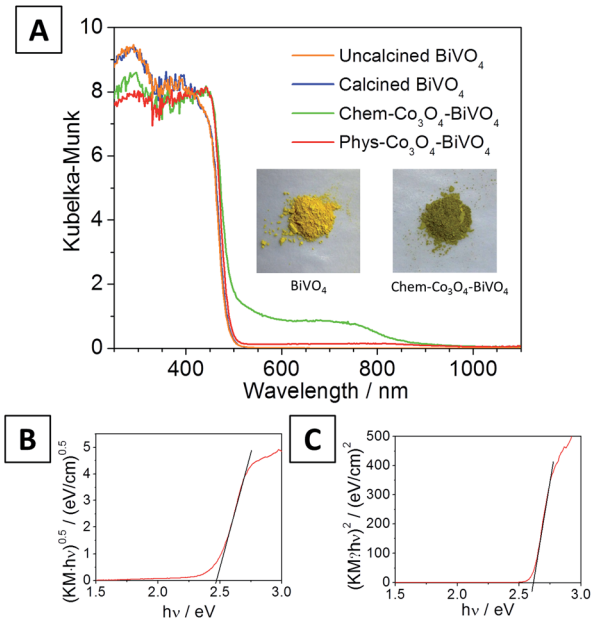

Fig. 2 UV-vis spectra and photos of $BiVO_4$ with cocatalysts (A) and Tauc plots for allowed indirect transitions (B) and direct transitions (C) of calcined $BiVO_4$.

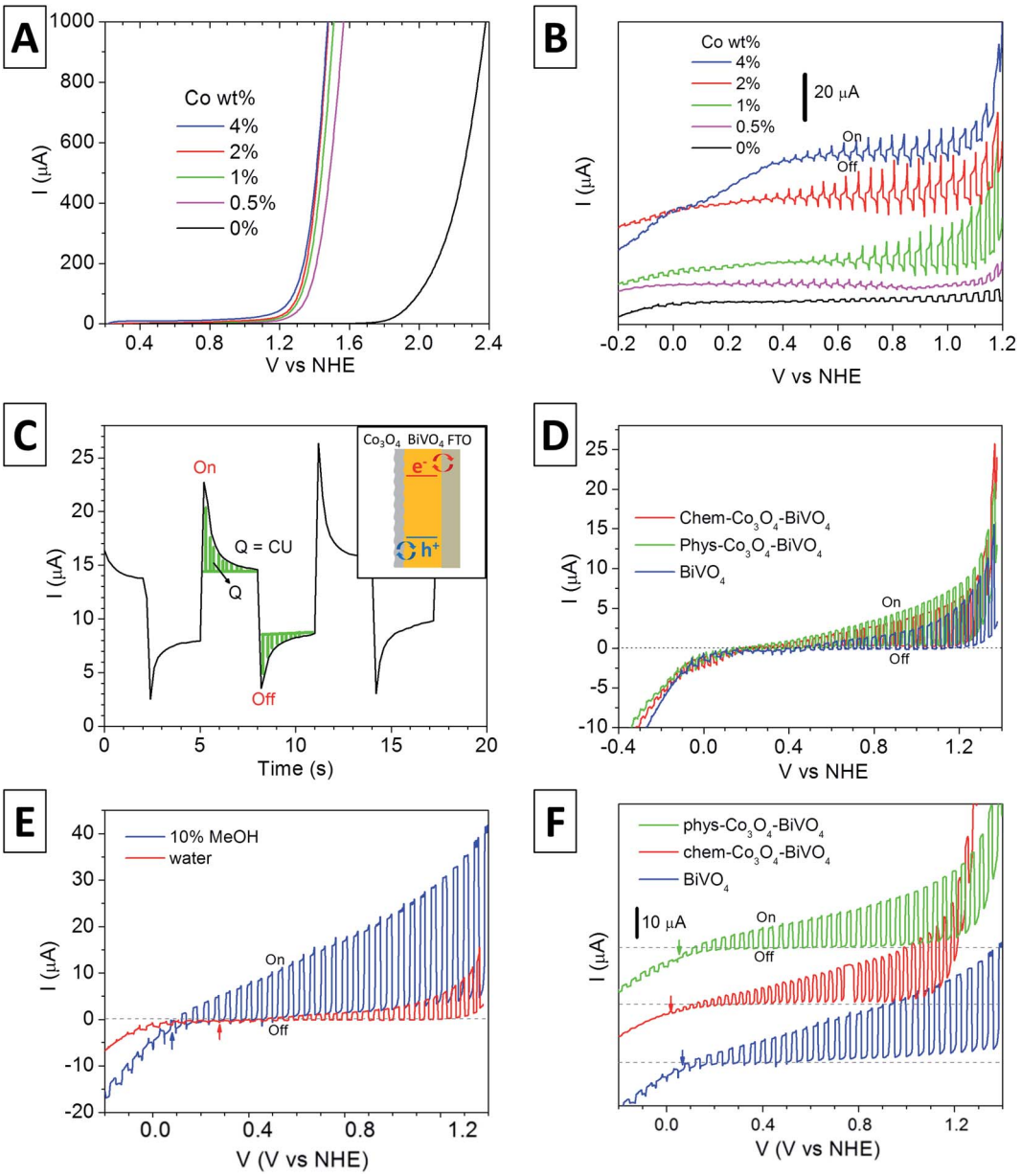

Fig. 3 (A) Dependence of overvoltage on Co_3O_4 content in dark, (B) photoelectrochemical scans of Echem-Co_3O_4–$BiVO_4$ with different amount of Co_3O_4, (C) capacitive current of 2 wt% Co Echem-Co_3O_4–$BiVO_4$ (0.9 V to 0.7 V, 10 mV s^{-1}), (D) photoelectrochemical scans of Phys-/Chem-Co_3O_4–$BiVO_4$ and $BiVO_4$, (A to D were measured in 0.1 M K_2SO_4 aqueous solution) (E) Comparison of photoelectrochemical scans of $BiVO_4$ in 0.1 M K_2SO_4 10 vol% methanol aqueous solution and water solution, (F) photoelectrochemical scans (0.1 M K_2SO_4 10 vol% methanol aqueous solution) of modified $BiVO_4$. (All electrodes are prepared with 0.5 mg catalyst on 1 cm^2 FTO substrate.)

an average rate of 1.24 mmol g^{-1} h^{-1}. The lower rate is a result of the lower illumination power (76 mW cm^{-2}, calculation in ESI†) under the conditions employed.

In order to further investigate charge transfer in the Co_3O_4–$BiVO_4$ composites, surface photovoltage spectroscopy (SPS) was employed.[26,27] Here, a contact-less Kelvin probe is used to record the light-induced changes in the contact potential as a function of the excitation energy (Fig. 5A). This can provide insight into photochemical charge transfer in solids,[28] at solid–solid[29] and solid–gas[30] interfaces, involving inorganic, molecular[31] and organic polymeric materials.[32] Because of its high sensitivity[30] it is possible to observe states with low optical cross sections, including trap sites in nanoparticles,[33] interfacial,[32] and defect states.[34] That makes the technique particularly useful for the study of nanoparticles.[30,35,36]

Spectra for nanoparticle films of Co_3O_4, $BiVO_4$, and Co_3O_4–$BiVO_4$ are shown in Fig. 5B. Under illumination $BiVO_4$ alone (blue) produces a negative signal with an onset at 2.45 eV and a maximum photovoltage of $\Delta CPD = -0.014$ V near 3.0 eV. This negative voltage indicates that electrons are moving towards the substrate and away from the Kelvin probe. The photoonset agrees with the optical band gap of the material, confirming

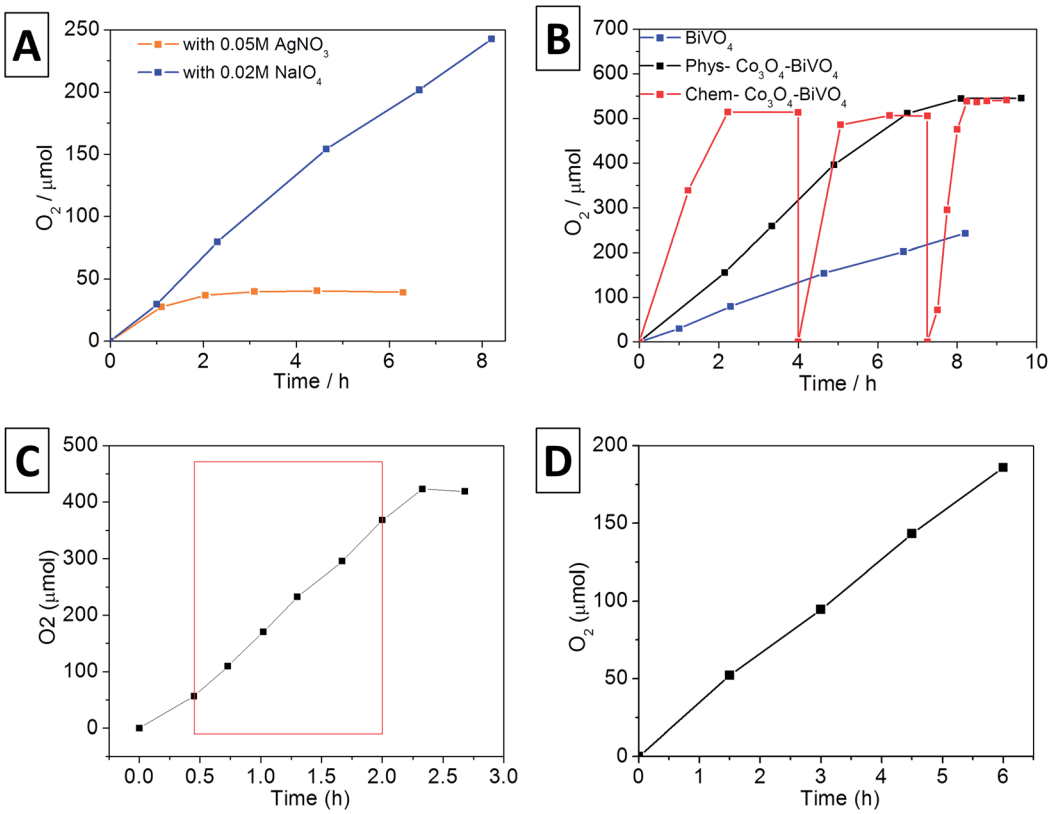

Fig. 4 Oxygen evolution from (A) $BiVO_4$ in 0.05 M aqueous $AgNO_3$ and 0.02 M $NaIO_4$ and (B) from $BiVO_4$, Chem-Co_3O_4–$BiVO_4$ and Phys-Co_3O_4–$BiVO_4$ in 0.02 M aqueous $NaIO_4$ (50 mg catalyst in 50 mL solution under light from Xe lamp at 380 mW cm^{-2} and with 400 nm long pass filter). (C) For the AQE measurement a 435 nm LED, 249 mW cm^{-2} by 2.54 cm^2 was used. (D) O_2 evolution from 25 mg Chem-Co_3O_4–$BiVO_4$ in 50 mL of 0.02 M aqueous $NaIO_4$ under sunlight.

that charge carriers are formed by band gap excitation. The spectrum for Chem-Co_3O_4–$BiVO_4$ (black) is similar, except that the curve has a steeper downward slope and the photovoltage is increased to −0.023 V at 3.0 eV. This indicates that the Co_3O_4 cocatalyst promotes hole accumulation in the film, likely through trapping on Co^{2+} sites. As a result, charge separation in the Co_3O_4–$BiVO_4$ system is improved. In contrast the photovoltage of Phys-Co_3O_4–$BiVO_4$ (red) is reduced compared to that for $BiVO_4$. This indicates that hole-trapping is less effective in this composite. The material also produces a positive CPD signal with a photoonset of 1.6 eV. This positive photovoltage signal below the $BiVO_4$ bandgap can be attributed to direct excitation of Co_3O_4. The spectrum for a pure Co_3O_4 film is shown in green. The 1.6 eV photoonset coincides with the onset of optical absorption of Co_3O_4 as seen at 800 nm (1.55 eV) in the optical spectrum in Fig. 2A. The positive sign indicates hole transport towards the substrate,[29] which agrees well with the p-type character of Co_3O_4.[37] The variable SPS behavior of Phys- and Chem-Co_3O_4–$BiVO_4$ shows that the electronic interactions between the Co_3O_4 and $BiVO_4$ components in both materials are different. While the physically mixed sample contains electronically isolated components, the chemically deposited sample supports selective hole injection from $BiVO_4$ into Co_3O_4. This suggests the formation of a p–n-heterojunction at the Chem-Co_3O_4–$BiVO_4$ interface. The photopotential of this junction can be estimated as the difference between the contact potential of the Chem-Co_3O_4–$BiVO_4$ sample and of the pure $BiVO_4$ and Chem-Co_3O_4 ($Co(NO_3)_2$ after 673 K calcination) components. At 3.0 eV, this value is (−23 mV)–(−14 mV)–3 mV = −12 mV. This voltage promotes water oxidation under illumination of Chem-Co_3O_4–$BiVO_4$. It is the reason for the higher photocatalytic activity of Chem-Co_3O_4–$BiVO_4$.

Lastly, the energetics of the Co_3O_4–$BiVO_4$ composites were analyzed to help understand the driving force for photocatalysis. To obtain quasi-Fermi levels of the materials, photoelectrochemical scans for $BiVO_4$ and Co_3O_4–$BiVO_4$ were recorded with methanol as fast hole acceptor (Fig. 3E and F). Under conditions of fast charge transfer at the solid–liquid interface, the photoonset potential is a good approximation of the quasi-Fermi level (electrochemical electron potential) of a semiconductor.[38] As can be seen from Fig. 3E, the addition of 10% methanol to the aqueous 0.1 M K_2SO_4 electrolyte increases the anodic photocurrent of the pure $BiVO_4$ film by a factor of 5, compared to the non-methanol case, and moves the onset potential 0.2 V into negative direction, to 0.1 V (NHE). In contrast, the photocurrents from Chem/Phys-Co_3O_4–$BiVO_4$ are only slightly enhanced by the methanol (Fig. 3F), and the negative shift of the onset potential is less than 0.1 V. This demonstrates that the performance of the composites is not limited by the water oxidation kinetics, but by other effects,

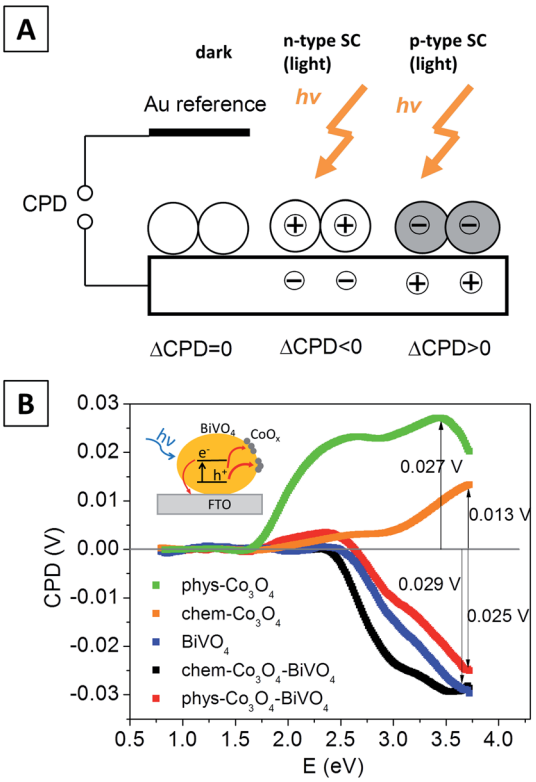

Fig. 5 (A) Surface photovoltage geometry, (B) surface photovoltage spectra of Phys-Co_3O_4, Chem-Co_3O_4, $BiVO_4$, and Chem/Phys-Co_3O_4–$BiVO_4$ (0.5 mg cm^{-2}) on FTO substrate in vacuum atmosphere (10^{-4} mbar), 175 W Xe lamp, 0.1 to 0.3 mW cm^{-2}.

including shading from Co_3O_4, and probably increased electron hole recombination from Co_3O_4–$BiVO_4$ interfacial states.

An energy scheme for the $BiVO_4$/Co_3O_4 photocatalytic system is shown in Fig. 6. The conduction band edge for $BiVO_4$ was calculated at 0.14 V *vs.* NHE by the method of Butler and Ginley[39] using the optical band gap from the Kubelka–Munk spectra and after correcting for the deviation from the point of zero charge to pH 7 (Details in ESI†). The valence band for this compound lies at 2.83 V *vs.* NHE. Similarly, with the 2.07 eV band gap of Co_3O_4,[40] conduction band edge and valence band edge of Co_3O_4 were calculated as 0.41 V and 2.48 V *vs.* NHE. From the anodic photocurrent onset of $BiVO_4$ (Fig. 4E and F) the quasi Fermi level of electrons, E_{Fn} is estimated around 0.1 V *vs.* NHE (from 10% MeOH it is 0.1 V and without methanol it is 0.3 V). This value is close to the conduction band, which agrees with the n-type character of $BiVO_4$.

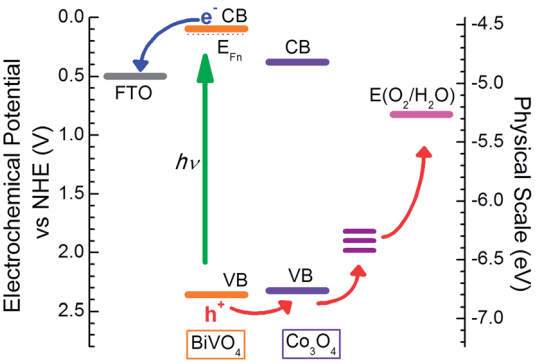

Fig. 6 Energy scheme of $BiVO_4$/Co_3O_4 photocatalytic system on electrochemical and physical scale at pH 7. Potential of $Co^{3+/2+}$ interfacial states estimated from $E^0(Co^{3+/2+}) = 1.92$ V.[24]

Based on the energy scheme in Fig. 6, the migration of light-induced electrons to the FTO support is possible, which is coherent with the SPV spectra. Addition of the Co_3O_4 phase allows photoholes to leave $BiVO_4$, causing the observed 12 mV increase in the photovoltage. Likely, the actual water oxidation reaction does not involve O states in the Co_3O_4 valence band, but intermediate $Co^{3+/2+}$ species at the Co_3O_4 surface. These states lower the water oxidation overpotential, but at the same time they act as recombination sites for electron hole pairs at the Co_3O_4–$BiVO_4$ interface. This is the reason for the low efficiency of the Co_3O_4–$BiVO_4$ junction and the small photopotential resulting from it. Similar junctions are likely present in single-crystal $BiVO_4$ composites reported recently by Li *et al.*[41]

Conclusions

In conclusion we have shown that the addition of cobalt oxide to powdered $BiVO_4$ improves the photocatalytic water oxidation ability of this system to 11 mmol g^{-1} h^{-1} O_2 from aqueous $NaIO_4$ solution under artificial visible light illumination (1240 μmol g^{-1} h^{-1} under sunlight) and an apparent quantum yield of 10% (at 435 nm). This activity ranks among the highest among known visible light driven water oxidation photocatalysts. Electrochemical measurements confirm that Co_3O_4 improves the water oxidation kinetics and lowers the overpotential. SPS confirms p-type character for the Co_3O_4 particles and a junction at the Co_3O_4–$BiVO_4$ interface. This junction improves electron–hole separation due to hole injection into Co_3O_4 and supports a photovoltage of ~12 mV at 3.0 eV. An analysis of the system energetics suggests that the activity of the catalyst can be improved further by eliminating mid gap states at the Co_3O_4–$BiVO_4$ interface that are responsible for electron hole recombination.

Experimental

Chemicals

Bismuth(III) oxide (99.9999% Acros Organics), vanadium(IV) oxide (99+% Strem Chemicals), cobalt(II, III) oxide (Puratronic 99.9985%, Alfa Aesar), cobalt(II) nitrate hexahydrate (98+%, Aldrich) and silver nitrate (99.9+%, Alfa Aesar) were used as received. Acetic acid (glacial, Macron) and nitric acid (68–70%, EMD) were used after proper dilution. Sodium metaperiodate (98%, Alfa Aesar) was used after recrystallization. Water was purified to 18 MΩ cm resistivity by a Nanopure II system.

Synthesis

$BiVO_4$ was synthesized *via* a revised solid-solution method[23] at room temperature. 1.15 g (2.5 mmol) of Bi_2O_3 and 0.42 g (5

mmol) of VO_2 were vigorously stirred in 25 mL 1 M aqueous acetic acid solution, at room temperature for 11 days. The obtained powder was washed with 50 mL of water for 3 times, then 50 mL of 0.5 M nitric acid and then again with 50 mL of water for 3 times. The washed powder was vacuum dried and calcined at 673 K for 5 hours in air.

Co_3O_4 was loaded by three different methods. In the first method, 200 mg $BiVO_4$ powder was soaked in 10 mL aqueous solution of 9.9 mg $Co(NO_3)_2 \cdot 6H_2O$ (equivalent to 2 mg of cobalt), and dried at about 353 K with slow stirring. The mixture was then calcined at 673 K for 5 hours. The obtained powder (Chem-Co_3O_4–$BiVO_4$) was washed with water and vacuum dried. In the second method, 200 mg $BiVO_4$ powder was ground together with 2.7 mg Co_3O_4 (equivalent to 2 mg of cobalt) for 10 minutes. The powder mixture was calcined at 673 K in air for 5 hours, washed with 50 mL of water and vacuum dried, to give Phys-Co_3O_4–$BiVO_4$ as a brown-yellow powder. Lastly, Echem-Co_3O_4–$BiVO_4$ was prepared as described in the main text.

Characterization

Transmission electron microscopy (TEM) images were taken with a Philips CM-12 TEM with accelerating voltage of 120 kV. To prepare the samples, copper grids with carbon film were dipped into aqueous dispersions of the catalysts, washed with pure water and dried in air.

Powder X-ray diffraction patterns were recorded with a Scintag XRD at the wavelength of 0.154 nm, with 2 mm tube slit divergence, 4 mm scatter, 0.5 mm column scatter and 0.2 mm receiving widths.

UV-Vis diffuse reflectance spectra were recorded on thin films using a Thermo Scientific Evolution 220 Spectrometer, equipped with an integrating sphere. To prepare the samples, the aqueous dispersions of the catalysts were drop-coated on white Teflon tape and then dried in air. The reflectance data were converted to the Kubelka–Munk function $f(R) = (1 - R)^2(2R)^{-1}$ to approximate absorbance.

Surface Photovoltage Spectroscopy (SPS) measurements were conducted using a vibrating gold Kelvin probe (Delta PHI Besocke) mounted inside a home-built vacuum chamber ($<1 \times 10^{-4}$ mbar). To prepare the samples, aqueous dispersions of 0.5 mg catalysts were drop-coated onto 1 cm^2 F/SnO_2 substrates (MTI Corporation, resistivity = 12–14 ohm $sq.^{-1}$), dried in air to form thin films and annealed at 673 K for 5 h. Samples were illuminated with monochromatic light from a 175 W Xe lamp filtered through an Oriel Cornerstone 130 monochromator and the light intensity range is 0.1 to 0.3 mW cm^{-2}. The CPD spectra were corrected for drift effects by subtracting dark scan background recorded prior to the light measurement. No correction for the variable light intensity from the Xe lamp was performed.

Photocatalytic oxygen evolution tests were performed by dispersing 50 mg of the catalysts in 50 mL 0.02 M sodium metaperiodate aqueous solution or 50 mL 0.05 M silver nitrate aqueous solution in a quartz glass flask. The flask was purged with argon several times and the solution mixture was irradiated with a 300 W xenon arc lamp using a 400 nm long pass filter (380 mW cm^{-2} at the flask surface as measured by an International Light IL1400BL photometer equipped with a GaAsP detector). The air-tight irradiation system was connected to a Varian 3800 gas chromatograph (with a 60/80 Å molecular sieve column and thermal conductivity detector) to measure the amount of evolved gases.

Photoelectrochemical measurements were conducted in a 3-electrode cell with a Pt counter electrode and a saturated calomel reference electrode connected to the cell with a KCl salt bridge. The cell was filled with 50 mL 0.1 M K_2SO_4. The solution was purged with N_2 to remove oxygen. The scans were recorded under 435 nm LED illumination (intensity 7.4 mW cm^{-2}) using a Gamry Reference 600 Potentiostat. For cyclic voltammetry scans, scans were performed in anodic direction with a rate of 10 mV s^{-1}. The cell was calibrated using the standard potential of $K_3[Fe(CN)_6]$ (+0.358 V *vs.* NHE). To prepare the working electrodes, 0.5 mg of the catalysts were drop-coated from aqueous dispersions on 1.0 cm^2 F/SnO_2 substrates (MTI Corporation, resistivity = 12–14 ohm $sq.^{-1}$), dried in air at room temperature and annealed at 673 K for 5 hours.

Acknowledgements

We are grateful for financial support from Research Corporation for Science Advancement (Scialog Award) and from the National Science Foundation (NSF, Grants 1152250 and 1133099).

Notes and references

1 F. E. Osterloh, *Chem. Mater.*, 2008, **20**, 35–54.
2 D. Yamasita, T. Takata, M. Hara, J. N. Kondo and K. Domen, *Solid State Ionics*, 2004, **172**, 591–595.
3 A. Kudo and Y. Miseki, *Chem. Soc. Rev.*, 2009, **38**, 253–278.
4 B. A. Pinaud, J. D. Benck, L. C. Seitz, A. J. Forman, Z. Chen, T. G. Deutsch, B. D. James, K. N. Baum, G. N. Baum, S. Ardo, H. Wang, E. Miller and T. F. Jaramillo, *Energy Environ. Sci.*, 2013, **6**, 1983.
5 F. F. Abdi, L. H. Han, A. H. M. Smets, M. Zeman, B. Dam and R. van de Krol, *Nat. Commun.*, 2013, **4**, 2195.
6 A. Kudo, K. Ueda, H. Kato and I. Mikami, *Catal. Lett.*, 1998, **53**, 229–230.
7 A. Kudo, K. Omori and H. Kato, *J. Am. Chem. Soc.*, 1999, **121**, 11459–11467.
8 S. Tokunaga, H. Kato and A. Kudo, *Chem. Mater.*, 2001, **13**, 4624–4628.
9 G. C. Xi and J. H. Ye, *Chem. Commun.*, 2010, **46**, 1893–1895.
10 M. C. Long, W. M. Cai and H. Kisch, *J. Phys. Chem. C*, 2008, **112**, 548–554.
11 D. N. Ke, T. Y. Peng, L. Ma, P. Cai and K. Dai, *Inorg. Chem.*, 2009, **48**, 4685–4691.
12 Y. Park, K. J. McDonald and K. S. Choi, *Chem. Soc. Rev.*, 2013, **42**, 2321–2337.
13 F. E. Osterloh, *Chem. Soc. Rev.*, 2013, **42**, 2294–2320.
14 S. K. Pilli, T. E. Furtak, L. D. Brown, T. G. Deutsch, J. A. Turner and A. M. Herring, *Energy Environ. Sci.*, 2011, **4**, 5028–5034.

15 S. K. Pilli, T. G. Deutsch, T. E. Furtak, J. A. Turner, L. D. Brown and A. M. Herring, *Phys. Chem. Chem. Phys.*, 2012, **14**, 7032–7039.
16 F. F. Abdi, N. Firet and R. van de Krol, *ChemCatChem*, 2013, **5**, 490–496.
17 F. F. Abdi and R. van de Krol, *J. Phys. Chem. C*, 2012, **116**, 9398–9404.
18 D. Wang, R. Li, J. Zhu, J. Shi, J. Han, X. Zong and C. Li, *J. Phys. Chem. C*, 2012, **116**, 5082–5089.
19 J. A. Seabold and K. S. Choi, *J. Am. Chem. Soc.*, 2012, **134**, 2186–2192.
20 S. P. Berglund, D. W. Flaherty, N. T. Hahn, A. J. Bard and C. B. Mullins, *J. Phys. Chem. C*, 2011, **115**, 3794–3802.
21 M. Long, W. M. Cai, J. Cai, B. X. Zhou, X. Y. Chai and Y. H. Wu, *J. Phys. Chem. B*, 2006, **110**, 20211–20216.
22 S. Trasatti, *J. Electroanal. Chem. Interfacial Electrochem.*, 1980, **111**, 125–131.
23 A. Iwase and A. Kudo, *J. Mater. Chem.*, 2010, **20**, 7536.
24 P. Vanysek, in *CRC Handbook of Chemistry and Physics*, CRC Press/Taylor and Francis, Boca Raton, FL, 2008.
25 A. R. Parent, R. H. Crabtree and G. W. Brudvig, *Chem. Soc. Rev.*, 2013, **42**, 2247–2252.
26 L. Kronik and Y. Shapira, *Surf. Sci. Rep.*, 1999, **37**, 1–206.
27 L. Kronik and Y. Shapira, *Surf. Interface Anal.*, 2001, **31**, 954–965.
28 M. K. Nowotny, P. Bogdanoff, T. Dittrich, S. Fiechter, A. Fujishima and H. Tributsch, *Mater. Lett.*, 2010, **64**, 928–930.
29 T. K. Townsend, N. D. Browning and F. E. Osterloh, *Energy Environ. Sci.*, 2012, **5**, 9543–9550.
30 J. Zhao and F. E. Osterloh, *J. Phys. Chem. Lett.*, 2014, **5**, 782–786.
31 P. Zabel, T. Dittrich, M. Funes, E. N. Durantini and L. Otero, *J. Phys. Chem. C*, 2009, **113**, 21090–21096.
32 F. E. Osterloh, M. A. Holmes, L. Chang, A. J. Moule and J. Zhao, *J. Phys. Chem. C*, 2013, **117**, 26905–26913.
33 M. Waller, T. K. Townsend, J. Zhao, E. M. Sabio, R. L. Chamousis, N. D. Browning and F. E. Osterloh, *Chem. Mater.*, 2012, **24**, 698–704.
34 R. Beranek, B. Neumann, S. Sakthivel, M. Janczarek, T. Dittrich, H. Tributsch and H. Kisch, *Chem. Phys.*, 2007, **339**, 11–19.
35 D. Gross, I. Mora-Sero, T. Dittrich, A. Belaidi, C. Mauser, A. J. Houtepen, E. Da Como, A. L. Rogach and J. Feldmann, *J. Am. Chem. Soc.*, 2010, **132**, 5981–5983.
36 F. A. Frame, T. K. Townsend, R. L. Chamousis, E. M. Sabio, T. Dittrich, N. D. Browning and F. E. Osterloh, *J. Am. Chem. Soc.*, 2011, **133**, 7264–7267.
37 C. S. Cheng, M. Serizawa, H. Sakata and T. Hirayama, *Mater. Chem. Phys.*, 1998, **53**, 225–230.
38 H. R. Sprunken, R. Schumacher and R. N. Schindler, *Faraday Discuss.*, 1980, **70**, 55–66.
39 M. A. Butler and D. S. Ginley, *J. Electrochem. Soc.*, 1978, **125**, 228.
40 A. Gulino and I. Fragalà, *Inorg. Chim. Acta*, 2005, **358**, 4466–4472.
41 R. G. Li, H. X. Han, F. X. Zhang, D. G. Wang and C. Li, *Energy Environ. Sci.*, 2014, **7**, 1369–1376.